Nuge, Tamrin ; Fazeli, Mahyar; Baniasadi, Hossein

Elucidating the enduring transformations in cellulose-based carbon nanofibers through prolonged isothermal treatment

Published in:
International Journal of Biological Macromolecules

DOI:
10.1016/j.ijbiomac.2024.133480

Published: 01/08/2024

Document Version
Publisher's PDF, also known as Version of record

Please cite the original version:
Nuge, T., Fazeli, M., & Baniasadi, H. (2024). Elucidating the enduring transformations in cellulose-based carbon nanofibers through prolonged isothermal treatment. *International Journal of Biological Macromolecules*, *275*(Part 1), Article 133480. https://doi.org/10.1016/j.ijbiomac.2024.133480

International Journal of Biological Macromolecules 275 (2024) 133480

Contents lists available at ScienceDirect

International Journal of Biological Macromolecules

journal homepage: www.elsevier.com/locate/ijbiomac

Elucidating the enduring transformations in cellulose-based carbon nanofibers through prolonged isothermal treatment

Tamrin Nuge [a,d], Mahyar Fazeli [b,*], Hossein Baniasadi [c]

[a] Department of Mechanical, Materials and Manufacturing Engineering, Faculty of Science and Engineering, University of Nottingham Ningbo China, 199 Taikang East Road, Ningbo 315100, China
[b] Department of Bioproducts and Biosystems, School of Chemical Engineering, Aalto University, FI-00076 Aalto, Finland
[c] Polymer Technology, School of Chemical Engineering, Aalto University, Espoo, Finland
[d] Center of Innovative Nanostructures & Nanodevices, University Technology Petronas, Malaysia

ARTICLE INFO

Keywords:
Biomass
Electrospinning
Electroconductive materials
Carbon nanofibers

ABSTRACT

This study investigates the conversion of highly acetylated sugarcane bagasse into high-modulus carbon nanofibers (CnNFs) with exceptional electrical conductivity. By electrospinning the bagasse into nanofibers with diameters ranging from 80 nm to 800 nm, a cost-effective CnNFs precursor is obtained. The study reveals the transformation of the cellulose crystalline structure into a stable antiparallel chain arrangement of cellulose II following prolonged isothermal treatment, leading to a remarkable 50 % increase in CnNFs recovery with carbon contents ranging from 80 % to 90 %. This surpasses the performance of any other reported biomass precursors. Furthermore, graphitization-induced shrinkage of CnNFs diameter results in significant growth of specific surface area and pore volume in the resulting samples. This, along with a highly ordered nanostructure and high crystallinity degree, contributes to an impressive tensile modulus of 9.592 GPa, surpassing that of most petroleum-based CnNFs documented in the literature. Additionally, the prolonged isothermal treatment influences the d002 value (measured at 0.414 nm) and CnNFs degree of crystallinity, leading to an enhancement in electrical conductivity. However, the study observes no size effect advantages on mechanical properties and electrical conductivity, possibly attributed to the potential presence of point defects in the ultrathin CnNFs. Overall, this research opens a promising and cost-effective pathway for converting sugarcane biomasses into high-modulus carbon nanofibers with outstanding electrical conductivity. These findings hold significant implications for the development of sustainable and high-performance materials for various applications, including electronics, energy storage, and composite reinforcement.

1. Introduction

In recent years, the pursuit of sustainable and high-performance materials has spurred interest in the conversion of cellulose-based nanofibers into carbon nanofibers (CnNFs) with exceptional properties. This transformation holds promise for addressing the growing demand for renewable and eco-friendly alternatives to conventional petroleum-derived materials in various applications. In particular, elucidating the enduring transformations undergone by cellulose-based precursors during prolonged isothermal treatment is critical for optimizing the synthesis of high-modulus CnNFs with enhanced electrical conductivity. Here, we present a comprehensive investigation into the conversion process of highly acetylated sugarcane bagasse into CnNFs, exploring the structural evolution and property enhancements resulting from prolonged isothermal treatment. Through electrospinning, we fabricate nanofibers with controlled diameters, serving as a cost-effective and sustainable precursor for CnNFs synthesis. Our study unveils the transition from cellulose to carbon, characterized by the formation of a stable antiparallel chain arrangement of cellulose II and a significant increase in carbon content. These insights not only contribute to a deeper understanding of the conversion mechanism but also pave the way for the development of sustainable and high-performance CnNFs for diverse applications.

CnNFs have garnered extensive research attention as nanostructured materials capable of creating macroscopic high-performance materials. Their advantageous characteristics, including low density, a low

---

* Corresponding author.
E-mail address: mahyar.fazeli@aalto.fi (M. Fazeli).

https://doi.org/10.1016/j.ijbiomac.2024.133480
Received 20 September 2023; Received in revised form 19 June 2024; Accepted 25 June 2024

coefficient of thermal expansion, high strength, stiffness, and customizable surface properties, make them ideal for various applications in aerospace, electronics, medical, sports, and housing. However, the widespread use and commercial adoption of CnNFs are currently hindered by critical challenges in the existing technology, such as high production costs, limited control over porosity and surface area for surface modification, as well as lower conductivity and mechanical properties compared to commercially available carbon fibers [1]. Li et al. developed flexible and self-supported highly porous carbon nanofibers (HPCNFs) using an electrospinning technique followed by a two-step carbonization process. Introducing air into the argon flow during carbonization resulted in partial combustion of the carbon nanofibers, creating numerous micro- and mesopores [2]. Bigdeli et al. successfully synthesized carbon nanofibers on the surface of activated carbon using a microwave-assisted chemical vapor deposition (CVD) method in a remarkably short time. This efficient and rapid approach produces nanofibers on ordinary activated carbon, significantly modifying its surface properties and enhancing its adsorptive capabilities for the deep desulfurization of liquid fuels [3]. Xing et al. developed a simple and reproducible method to synthesize mesoporous carbon nanofibers (MCNFs) using dual hard templates: a porous anodic aluminum oxide (AAO) membrane and colloidal silica (Ludox TM-40). By simultaneously removing AAO and silica, the process is streamlined. Using phenol resin as the carbon precursor, the resulting MCNFs feature a high surface area, mesoporous volume, and a hierarchical nanostructure with hollow macrochannels, large mesopores (about 22 nm), and micropores [4]. Magana et al. prepared high-surface-area carbon nanofibers (820 m^2/g) using a nanocasting approach with silica nanofibers derived from chromonic liquid crystals as a template. These CNFs, featuring randomly oriented graphitic layers, demonstrated excellent electrochemical supercapacitance performance [5]. To tackle these limitations, electrospinning technology has been proposed as a cost-effective and straightforward technique for fabricating CnNFs in the range of 80 to 700 nm, providing excellent control over morphology, composition, and porosity [6]. In recent years, the pursuit of sustainable and high-performance materials has spurred interest in the conversion of cellulose-based nanofibers into carbon nanofibers (CnNFs) with exceptional properties. This transformation holds promise for addressing the growing demand for renewable and eco-friendly alternatives to conventional petroleum-derived materials in various applications. Previous studies have demonstrated the feasibility of fabricating CnNFs from biomass-derived precursors, showcasing the potential of sustainable feedstocks in carbon nanofiber synthesis [7–10].

Synthetic polyacrylonitrile (PAN) is widely regarded as the gold standard for CnNFs manufacturing due to its high melting point and substantial carbon yield [11,12]. The electrospinning process has successfully produced PAN-based CnNFs with diameters below 100 nm [13,14]. PAN's thermal stability makes it a superior precursor, allowing researchers to tailor strength and modulus through carbonization processes [15]. However, the high cost of PAN precursors constitutes nearly half of the production expenses, highlighting the urgent need for more affordable, renewable, and environmentally friendly alternatives [16,17].

To address these challenges, researchers have actively sought alternative carbon nanofiber precursors that are cost-effective and sustainable. Studies have shown that biomass, such as cellulose, holds promise as a potential precursor, as it reduces precursor costs, energy consumption, and greenhouse gas emissions (CO2 equivalents) by approximately 22 %, 5 %, and 13 %, respectively, compared to PAN [18,19]. Therefore, cellulose from sugarcane bagasse has been suggested as a novel biobased precursor for carbon nanofiber fabrication. However, due to the high crystallinity and extensive hydrogen bonding of cellulose, conventional electrospinning methods are not feasible for cellulose [20–24]. In this work, an acetate ester of cellulose derived from sugarcane bagasse has been introduced as a precursor to obtaining porous nanoarchitecture CnNFs with controlled morphology and porosity. Notably, a systematic optimization of the electrospinnability of high acetyl-content cellulose acetate has not been reported in the literature.

In this study, we hypothesized that high-yield carbon nanofibers with outstanding mechanical properties and electrical conductivity could be prepared from carbohydrates, such as sugarcane biomasses. While most studies on CnNFs pyrolysis focus on optimizing the carbonization process by controlling temperature and heating rate variability [20–22], the novelty of our work lies in exploring the effect of isothermal stabilization temperature on improving precursor conversion into CnNFs. We evaluated the impact of different isothermal stabilization temperatures on cellulose nanofiber precursor's structure, yield, surface area, and mechanical and electrical properties. Through systematic isothermal optimization, the cellulose nanofiber precursor underwent structural changes, resulting in a highly porous and interconnected uniform carbon nanofibrous network. Detailed investigations of the structures and properties of the cellulose nanofiber after the isothermal treatment and carbonization process were conducted. The thermal treatment opened new avenues for manipulating carbon nanofiber structures and morphologies to fabricate high-performance nanoscale building blocks.

2. Materials and methods

2.1. Materials

Cellulose acetate (CA) (acetyl content 42.8 %, M_W = 300,000), derived from bio-waste sugarcane straw and bagasse, was provided by Anhui Taicheng Paper and Plastic Technology Co., Ltd., Qingdao, China. The solvents, including 1 M NaOH, 99 % ethanol, dimethylacetamide, and acetone, were purchased from Sigma Aldrich. All the chemical reagents used in this study are completely dried in an oven at 50 °C for 24 h to avoid any possible influence of water.

2.2. Electrospinning solutions preparation

Cellulose acetate solutions were meticulously prepared by dissolving varying amounts of cellulose acetate in different working solvents (as shown in Table 1). The cellulose acetate concentrations ranged from 8 % to 25 % (*w/v*). Subsequently, the solutions' physical properties and electrospinnability were investigated through measurements of viscosity, surface tension, and conductivity. These crucial analyses shed light on the characteristics of the as-prepared solutions, providing valuable insights for the subsequent electrospinning process [25].

2.3. Electrospinning

The experimental setup for electrospinning involved an adjustable DC power supply capable of generating DC voltage ranging from 0 to 30 kV. A 10 mL syringe, connected to a stainless-steel spinneret with an outer diameter of 1.27 mm and an inner diameter of 0.838 mm, was precisely controlled by an automatic syringe pump obtained from New Era Pump Systems Inc., USA. The collection process utilized a square aluminum plate measuring 11 × 11 cm covered with aluminum foil, functioning as the grounded collector. The distance between the spinneret's tip and the collector was consistently maintained at 10 cm.

To initiate the electrospinning process, the cellulose acetate solution was continuously fed at a rate of 0.3 mL/h. The blunt end of the spinneret was charged with positive polarity of 15 kV DC voltage from the power supply. For safety purposes, all experimental procedures were conducted within a dedicated chamber equipped with a safety mechanism. Moreover, a dedicated forced ventilation system was installed above the chamber to effectively capture and eliminate any evaporated volatile substances from the experimental setup. The entire electrospinning process was carried out at room temperature, and the resulting electrospun scaffolds were left to dry overnight in a dry cabinet before undergoing subsequent analysis.

Table 1
Electrospinnability of cellulose acetate (CA) in single and binary solvent systems (DmAC: Dimethylacetamide; AA: Acetic Acid; DCM: Dichloromethane. *Diameter of most frequent fiber).

Solvent	Conductivity (mS/cm)	Surface tension (mN/m)	Viscosity (Pa.s)	*Diameter (nm)	Fiber formation
Acetone	58.69 ± 0.405	48.41 ±1.027	2.641	–	Un-spinnable gel formation during the electrospinning
DmAc/ Acetone (1:2)	56.33 ±0.092	46.35 ±0.493	3.420	97 ± 0.943	Nanofibers with beads
AA/ ddH$_2$O (3:1)	57.53 ±0.110	62.39 ±0.947	6.654	–	Un-spinnable. Gel formation
DCM/ Acetone (3:1)	52.96 ±1.230	25.36 ±0.866	2.740	25 ± 0.641	Beads

2.4. Optimizing the CA in DmAC: acetone solvents compositions

The electrospinnability of CA in DmAC: Acetone binary solvents was thoroughly investigated by dissolving varying amounts of cellulose acetate powder in different DmAC: Acetone compositions. The concentration of CA ranged from 2 % to 35 % (*w/v*). To identify and predict the electrospinnability domains based on solution compositions and resultant morphologies, a pseudo-ternary phase diagram was constructed using the procedure established by Ago et al. [26]. The composition of the solutions was typically described in terms of the mass fraction (Fi) of the individual components, calculated using Eq. (1), where mi represents the mass of each constituent in the solution (CA, Acetone (Ace), or DmAc):

$$F_i = \frac{m_i}{m_{Ace} + m_{CA} + m_{DmAc}} \tag{1}$$

The resulting CA nanofibers with desired diameter size were categorized into 3 different criteria: ultrathin (average diameter = 80 nm), thin (average diameter = 200 nm), and thick (average diameter = 400).

2.5. Deacetylation of the CA nanofiber

The CA nanofibers underwent deacetylation in a 0.5 N NaOH ethanol solution at 25 °C, allowing the process to occur overnight. Fig. 1 represents the main processing steps for cellulose-based carbon nanofiber. The resulting cellulose nanofibers (CNFs) were then thoroughly washed with deionized distilled water five times. Subsequently, the nanofibers were labeled based on their diameter size as ‘CNF_18’ (ultrathin), ‘CNF_23’ (thin), and ‘CNF_25’ (thick) before undergoing further analysis.

2.6. Stabilization and carbonization

To prevent the CNFs from losing their shape during the thermal treatment, they were securely fixed on graphite bridges while undergoing the stabilization process. The nanofibers were stabilized in an air atmosphere (7 L/min) using a KSL-1200× muffle furnace (MTI Corporation, USA). The temperature was gradually increased from 25 to 250 °C at a rate of 1.0 °C/min, followed by an isothermal treatment for 1 h, 5 h, and 10 h, respectively. The resulting oxidized CNFs were labeled as ‘CNF_1’, ‘CNF_5’, and ‘CNF_10’, corresponding to their respective isothermal times.

Subsequently, the treated cellulose nanofibers underwent a carbonization process in a similar tubular furnace under a continuous nitrogen flow of 200 mL/min. The heating rate was set to 1 °C/min until reaching 600 °C, followed by 3 °C/min until reaching 800 °C. After the carbonization, the samples were allowed to cool down naturally to room temperature under continuous nitrogen flow, with the entire process taking approximately 4 to 5 h [27]. The yield of carbon content from the carbonization process was determined by subtracting the original dried stabilized sample mass from that of the final carbon product. The resulting carbon nanofibers (CnNFs) were then labeled as ‘CnNF_1’, ‘CnNF_5’, and ‘CnNF_10’, indicating their precursor isothermal treatment times.

2.7. Morphology and structural properties of CA nanofibres and CnNFs

The morphology of nanofibers was analyzed using Zeiss SIGMA VP (Zeiss, Germany) scanning electron microscopy (SEM) at an accelerating voltage of 5 kV. Prior to the SEM observation, a small section of the nanofiber mat was carefully cut at three distinct positions. These cut sections were then affixed to the sample holder using double-sided

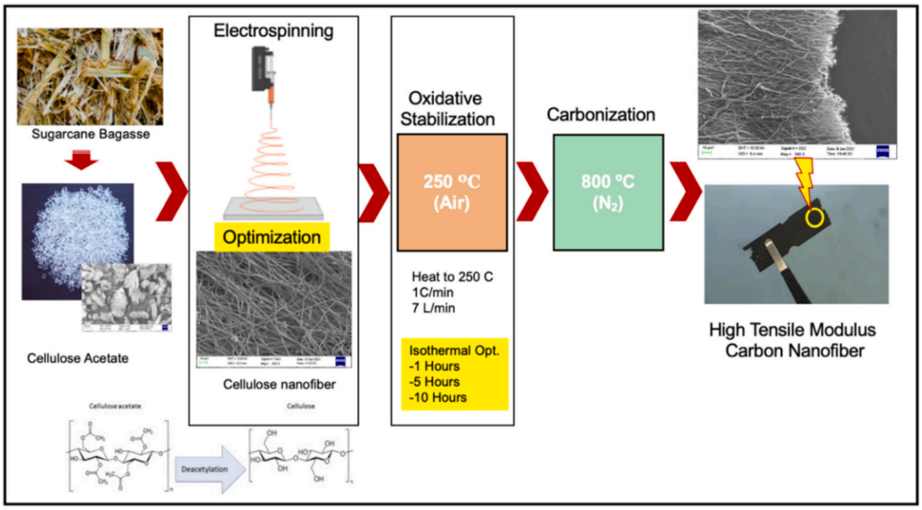

Fig. 1. Main processing steps for fabricating of high tensile modulus cellulose-based carbon nanofiber.

carbon tape. This preparation allowed for the subsequent examination of the nanofiber samples under the SEM. The samples were then coated with a 4 nm gold layer under an argon atmosphere using Leica EM SCD500 (Leica, Germany) high vacuum gold sputter [28]. Typically, 100 nanofibers at different positions were measured and analyzed using ImageJ software developed by the Upper Austria University of Applied Sciences. Elemental compositions (wt%) of the nanofibers were determined by energy dispersive X-ray analysis (Oxford Instrument, UK) at an acceleration voltage of 15 kV, using a working distance of 10 mm and a BSE detector.

Further elemental analysis of samples was performed using CHNS elemental analyzer (Elementar, Germany) to quantify the carbon, hydrogen, nitrogen, and sulfur contents. The CHNS analysis was conducted utilizing the Pregl-Dumas technique with a furnace temperature of 1100 °C. The samples were completely combusted in the presence of an excess of oxygen, and any NOx gases present were reduced to N_2 during the analysis process. The product gases, including H_2O, CO_2, SO_2, and N2, were collected in a mixing chamber and thoroughly mixed before undergoing separation. Gas chromatography with thermal conductivity detection was employed for the separation and analysis of the gases. The obtained results were reported as weight percentages of each element, with a limit of detection below 0.10 %.

Fourier transform infrared (FTIR) spectra ranging from 4000 to 400 cm^{-1} were obtained using a Bruker Vertex 70v FTIR spectrometer equipped with an attenuated total reflectance (ATR) accessory. To conduct the measurements, a thin layer of the nanofiber mat was applied onto the ATR crystal with a thickness (d) of 2 mm, and constant pressure was applied to ensure proper contact. The spectra were acquired by performing 16 scans at a spectral resolution of 4 cm^{-1} and subsequently subjected to baseline correction. The reported spectra represent an average of three separate measurements.

The X-ray diffraction (XRD) analysis was used to analyze the changes in the phase structure of the nanofiber samples. The diffractometer with CuKα radiation was operated at 20 kV tube voltage and 110 mA tube current at 2θ range of 5° - 40° with a step size of 0.02° using a copper anode as the target.

Thermogravimetric analysis (TGA) was performed on TGA Q600 SDT (TA Instrument, USA) in a nitrogen atmosphere (flow rate 50 mL/min) at 10 °C/min heating rate ramped from 30 °C to 1000 °C. Before analysis, 20 mg of the sample was weighed and placed in a ceramic crucible.

The nanofibers' specific area and pore size were examined using ASAP 2020 (Micromeritics, USA). Before the test, the sample was degassed for 10 h under vacuum conditions. Nitrogen adsorption-desorption isotherms were recorded at 90 °C. The Brunauer-Emmett-Teller (BET) theory was employed to derive the specific surface area from the linear region of the BET plot. The micropore size distribution and micropore volume were determined from the T-plot method. The mesopore size distribution (adsorption and desorption) and mesopore volume (adsorption) were calculated using the Barrett, Joyner, and Halenda (BJH) method.

2.8. Tensile testing

The mechanical properties of the carbon nanofiber were evaluated using an MTS Exceed® Series E42 universal tensile tester (manufactured by MTS, China), which was equipped with a 1 kN load cell. The tests were performed in accordance with the ASTM Standard D882–12, which specifies the standard test method for determining the tensile properties of thin plastic sheeting. Each sample was prepared by cutting it into strips measuring 90 × 10 mm, with a gauge dimension of 10 × 50 mm. The thickness of the samples was controlled within the range of 350 μm by adjusting the electrospinning time. Tensile tests were conducted at a crosshead speed of 10 mm/min and a preload of 0.1 MPa, both at room temperature. The reported values for tensile strength and tensile stress represent the average of six separate measurements.

2.9. Electrical characterization

The electrical properties of the carbon nanofiber mats were assessed under DC voltage. Square-shaped specimens with dimensions of approximately 2 mm thickness and 20 × 20 mm were utilized for the DC volume conductivity measurements. Before conducting the electrical measurements, the samples were subjected to a thermal pre-treatment at 90 °C for 10 h to eliminate any residual moisture or solvents. Subsequently, both sides of the samples were coated with a silver paste to minimize the impact of surface roughness and ensure the establishment of Ohmic contacts.

3. Results and discussion

3.1. Electrospinnability cellulose acetate solutions from sugarcane bagasse

Table 1 provides a summary of the spinning performance of cellulose acetate derived from sugarcane bagasse in various solvent systems, along with a comparison to the literature review. It is important to note that when cellulose acetate was dissolved in acetone and acetic acid/water binary solvents, gelation occurred during the electrospinning process. This gelation phenomenon can be attributed to the intensified polymer-polymer and polymer-solvent interactions induced by the applied electric field.

The higher degree of acetyl groups in the cellulose acetate obtained from sugarcane bagasse is likely to interact more strongly with the carbonyl group in acetone. The proton-donating ability of the acetyl content induces dipole-dipole interactions in the presence of an electrostatic field, leading to the aggregation of CA-acetone during electrospinning (Fig. 2a) [29]. As shown in Table 1, the high acetyl group content in the CA synthesized from sugarcane bagasse results in a highly conductive CA dissolution. Previous studies by Kawabata and Matsuo [30] reported poor electrorheological properties in natural polymers with low acetyl group content due to low proton conductivity in the mixture. In contrast, Angel et al. [31] successfully electrospun non-aggregated CA dissolution with smooth, uniform CA nanofibers by employing CA with a low acetyl group content during the electrospinning process.

On the other hand, the gelling effect of CA in acetic acid/water binary solvents is intensified by the high acetyl degree, promoting the formation of water bridges between hydrogen bonds in water molecules. As acetic acid evaporates over time, the intermolecular interaction between acetyl and water intensifies, leading to aggregation and the formation of induced structure gels [32]. To mitigate this effect, Appaw et al. [33] suggested that adding very low water content could inhibit gel formation and improve the CA electrospinnability in the AA/water binary solvent system. Consequently, smooth nanofibers with an average diameter of 180 nm were obtained from a CA concentration of 17 % dissolved in an AA/water system with a low water ratio (as shown in Table 1) [34]. However, in our study, even with a meager water ratio, the CA still exhibited gel formation during the mixing process. The phenomenon of gel transition at low water content remains not well understood in our case. Nevertheless, the occurrence of physical gelling at low non-solvent (water) presence is intriguing, particularly in membrane preparation [35].

The addition of DmAC and DCM into the acetone binary solvents effectively inhibits the gelation effect during the electrospinning process. However, the presence of DmAC and DCM may induce a negative dielectric anisotropy, disrupting the electrorheology effect in the DmAC/Acetone and DCM/Acetone binary solvent systems during electrospinning [36] (Fig. 2a), which prevents the gelling effects. Despite exhibiting better dissolution behavior, the electrospinning of CA in DCM/Acetone resulted in the formation of dense, large beads adhered along the fine nanofibers (Fig. 2b). This observation can be attributed to inadequate chain entanglements in the polymeric solution [37], as evident from the low viscosity reading (Table 1). The combination of

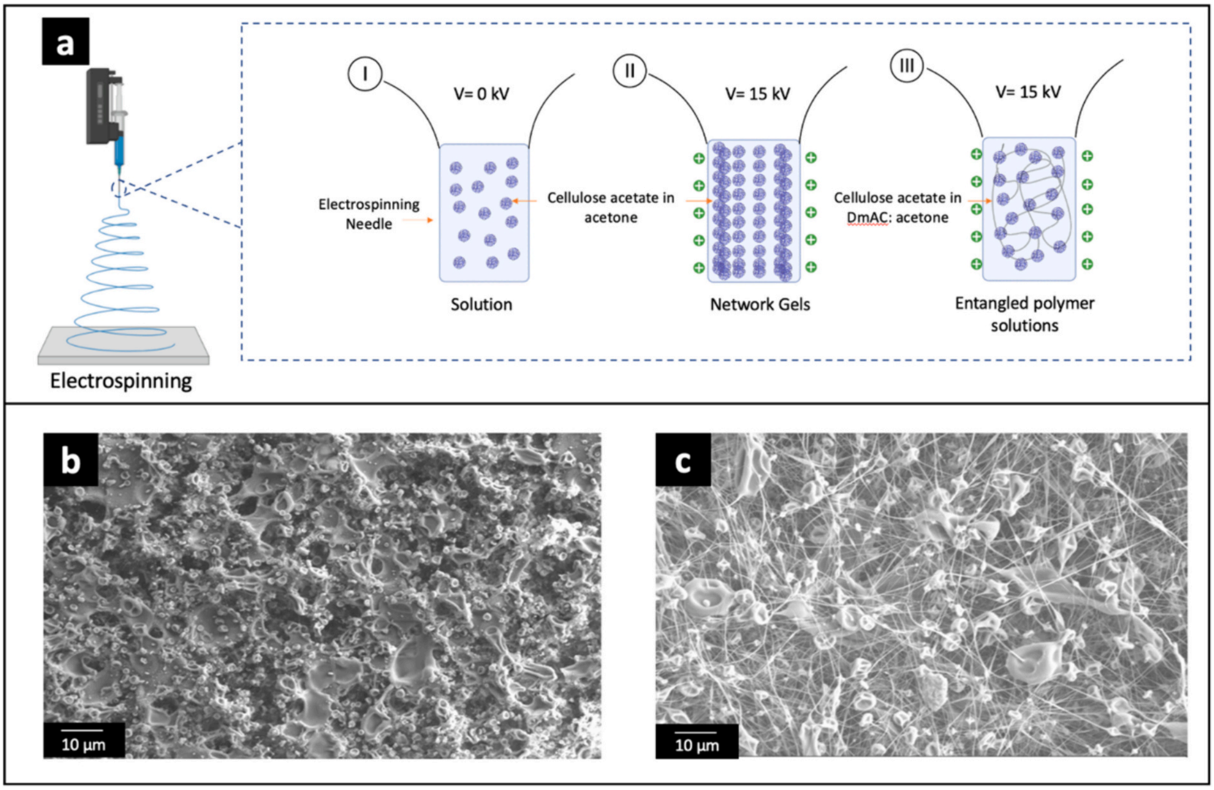

Fig. 2. (a). Structural patterns of high acetyl content of cellulose acetate during the electrospinning process. Enlarge schematic images (I). The dispersion of the CA in the acetone without an electric field influenced (II). Model orientation of chain-like structure of CA in acetone turned into electrorheology fluid under electric field influenced. (III). Model orientation of entangled CA polymer solutions in DmAC/Acetone binary solvents during the electrospinning. Scanning electron micrographs of electrospun cellulose acetate derived from sugarcane bagasse in different solvent systems (b). DCM: Acetone (1:1) (c). DmAC: Acetone (1:2). The SEM micrographs for nanofibers domains were magnified at 1000× with scale Bar = 10 µm.

low viscosity and high solution surface tension likely led to jet breakage during the electrospinning of CA in this solvent system, resulting in the formation of beads along with a distinct amount of very fine nanofibers.

Conversely, more pronounced nanofibers with an average size of 90 nm were obtained from the electrospinning of CA solutions in DmAC/Acetone (Fig. 2c). Similarly, beaded nanofibers were observed in this case, attributed to the inadequate CA concentration and low solution viscosity. The formation of beads is expected whenever surface tension forces overcome the polymeric solution's charge repulsion and viscoelastic forces. The occurrence of Rayleigh instability in the fluid jet, caused by the low viscoelasticity of the solution, can lead to jet breakup into droplets. However, increasing the concentration of the polymer solution enhances its elasticity, suppressing Rayleigh instability and promoting the formation of nanofibers without the presence of beads [38]. The subsequent section of this study aims to investigate the relationship between the high acetyl content of CA-DmAC-Acetone on nanofiber morphology. This investigation will help establish electrospinnability boundaries that can predict the characteristics of the as-obtained nanofibers.

3.2. Electrospinnability boundaries of cellulose acetate in DmAC: acetone binary solvent system

The data obtained from the electrospinning process, along with the influence of mixed solvent composition on the average diameter of the cellulose acetate (CA) nanofibers, were plotted in a ternary diagram (Fig. 3). This approach was employed to identify electrospinnability domains and predict the diameter of the electrospun fibers. A similar ternary diagram was successfully used by Erencia et al. [39] to predict electrospinnability zones and nanofiber sizes for gelatin nanofibers.

In our study, the ternary diagram effectively represented the data from the electrospinning process and nanofiber diameters, enabling the identification and prediction of electrospinnability domains and composition regions. This facilitated the assessment of the feasibility of different solvent compositions. By considering the electrospinnability boundaries, it became possible to predict fiber morphologies in relation to the solution composition, represented as a mass fraction (Fi). Within the ternary diagram, shifting the composition along the vertical line indicates alterations in the content of DmAC. As the composition approaches the DmAC apex in the diagram, the concentration of DmAC increases. Conversely, changes in the horizontal direction closer to "cellulose acetate" indicate variations in the concentration of cellulose acetate.

3.2.1. Solidified region

In this particular area, solutions with high viscosity were obtained, and the electrospinning process ultimately failed. The solidification of the mixtures occurred when the FCA values exceeded 0.30, indicating the solubility limit of cellulose acetate [75]. Le et al. [40] reported a much lower solubility limit of cellulose acetate in 1-ethyl-3-methylimidazolium acetate EmimAc, with very slow dissolution kinetics observed in 25–27 % (*w*/*v*) cellulose acetate. To accelerate the dissolution, the CA mixture was stirred at an elevated temperature.

3.2.2. Electrospray region

Within this specific domain, the solutions failed to generate a continuous jet during the electrospinning process, resulting instead in a spray-like dispersion onto the collector surface. This phenomenon can be attributed to the insufficient viscoelastic force within the jet, which is unable to maintain a fibrous structure. From a compositional perspective, this region corresponds to the minimum concentration of cellulose acetate required for proper dissolution and electrospinnability. It is

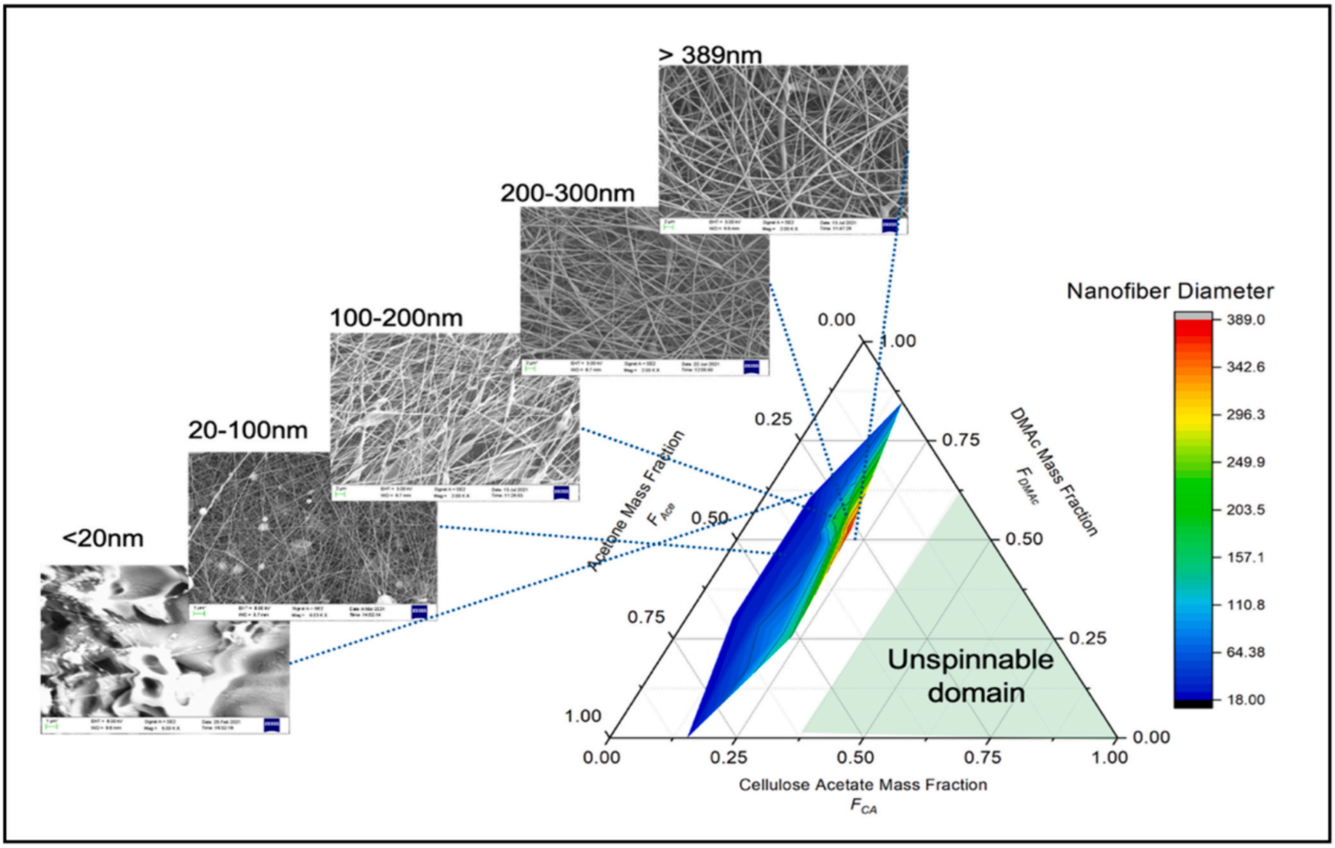

Fig. 3. Ternary diagram showing the electrospinnability domains and contour lines for different nanofibers domains based on the composition of the precursor solution (Cellulose acetate (FCA), DMAc (FDMAc), and acetone (FAce) mass fraction). The SEM micrographs for nanofibers domains were magnified at (>100 nm Mag. 2000× with scale Bar = 2 μm; < 100 nm Mag. 5000× with scale Bar = 1 μm).

noteworthy that at lower CA concentrations, chain entanglement was inadequate to achieve the minimal viscoelastic force necessary for an electrospinning jet. Therefore, the threshold FCA value required to transition from electrospraying to electrospinning was higher than 0.05.

Moreover, electrospinnability necessitated FAA values up to 0.7. Similarly, Han et al. [32] reported that a higher concentration of aqueous acetic acid, up to 75 %, was necessary for the electrospinnability of CA nanofibers. With a higher acetic acid concentration, the opportunities for polymeric chain entanglement increased due to the expansion of the cellulosic chains [41]. Nevertheless, cellulose acetate concentration remains the limiting factor in electrospun CA fabrication, requiring a minimum CA concentration threshold value for successful electrospinning.

3.2.3. *Beaded fibers region*

The formation of beaded fibers was attributed to the lack of chain entanglements. In this study, beaded fibers were observed in regions defined by the following conditions: $0.08 < \mathrm{FCA} < 0.38$, FAce <0.4, and $0.6 <$ FDmAc <0.9. It is noteworthy that beaded fibers were predominantly produced at low acetic acid concentrations. At these lower acetic acid levels (FAce <0.4), the expansion of cellulosic chains likely did not occur, leading to a higher likelihood of the electrospinning jet breaking up into droplets and resulting in bead formation.

3.2.4. *Bead-free fibers region*

After delineating the aforementioned regions, the remaining area encompassed all the solutions that exhibited the formation of both nanofibers and microfibers. Smooth microfibers could be attained within the following conditions: $0.2 < \mathrm{FCA} < 0.3$ and $0.52 <$ FDmAc <0.7. Meanwhile, smooth nanofibers were attainable in the regions that satisfied the following conditions: $0.05 < \mathrm{FCA} < 0.2$ and $0.62 <$ FDmAc <0.9. The diameter of the electrospun fibers was found to increase with the increase in cellulose acetate concentration.

Based on the obtained results, nanofibers and microfibers with diameters ranging from 54 nm to 800 nm were successfully produced within these domains. Notably, the electrospinnability domain for smooth electrospun CA nanofibers fell within the optimum DmAC/Acetone range for CA electrospinnability. For carbon nanofiber production, cellulose acetate nanofibers with different sizes (80 nm, 200 nm, and 400 nm) were prepared by adjusting the mass fraction of the solution's components. Consequently, nanofibers with diameters of 80 nm, 200 nm, and 400 nm were successfully fabricated and utilized as precursors for carbon nanofiber production.

3.3. *Effect of isothermal treatment on structural changes and crystallinity properties*

In this study, the effect of isothermal dwelling time on the structural and crystallinity changes of cellulose nanofibers was systematically investigated for the first time. Generally, isothermal stabilization induces changes in cellulose precursors through processes such as dehydration, oxidation, crosslinking, and cyclization [42]. Fig. 4a presents the FTIR spectra of the cellulose nanofibers after undergoing stabilization at temperatures ranging from 25 to 250 °C, with a heating rate of 1.0 °C/min, and various isothermal times (0, 1, 5, and 10 h) at 250 °C. It has been reported that oxidative stabilization temperatures above 250 °C can cause deterioration in the cellulose crystal structure [43]. Therefore, 250 °C was selected as the optimal temperature for cellulose oxidative stabilization. Prolonged oxidative time at 250 °C is essential to promote changes in cellulose crystallinity [44], although longer

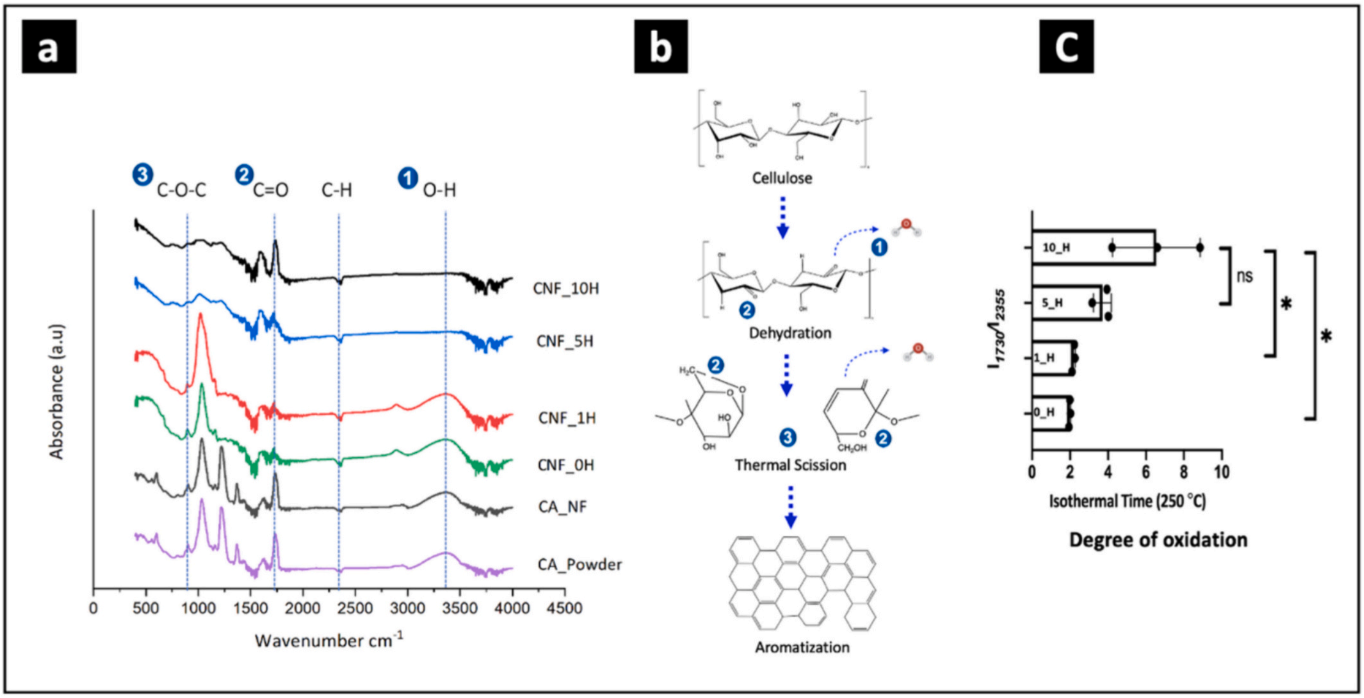

Fig. 4. (a). FTIR spectra of cellulose acetate NF, cellulose NF and different isothermal treatments of cellulose NF (b). Mechanisms of stabilization chemistry and structure of the stabilized cellulose nanofiber according to [46]. (c). Oxidation degree (I1730/I2355) from FTIR spectra as a function of isothermal time at 250 °C.

isothermal treatment for >16 h may result in modulus losses in the sample [45].

A continuous and distinct reduction in the O—H stretching band intensity between 3000 and 3600 cm-1 was observed after a longer isothermal dwelling time of >1 h. This decrease in the O—H stretching band can be attributed to dehydration activity during the stabilization process [46] (Fig. 4b). Additionally, the degradation of aliphatic compounds, such as methyl and methylene functionalities in cellulose, due to thermal scission, explains the disappearance of intensity in the region between 2820 and 2950 cm^{-1} and the C—O stretching band at 893–1105 cm^{-1}. Furthermore, the thermal scission induced the formation of unconjugated ketones, carbonyls, and ester groups (Fig. 4b) [47], with the presence of oxygen from the air, as evidenced by the increased intensity of the signal related to the oxidation C═O stretching at 1730 cm^{-1}. The high signal intensity of the CA powder and CA nanofiber is attributed to the presence of the acetyl group in the CA. Notably, a distinct C═O stretching band was observed only after 5 h of dwelling time, indicating that the oxidation reaction occurred only during longer isothermal times.

Structural changes, such as the formation of extensive aromatic domains on the cellulose nanofibers, were observed after 5 h of isothermal treatment, as evidenced by a distinct band at 1770–1750 cm^{-1}. The presence of a high aromatic network structure (Fig. 4b) was further verified by the disappearance of the band at 750 cm^{-1}, which is related to the loss of oxygen functionality of cellulose due to the formation of fused ring systems. This transformation into a thermoset state via the fused ring systems enhances the carbon yield during the carbonization process.

The evaluation of structural changes in cellulose nanofibers can be extended by estimating the oxidation degree (OD) through the measurement of the intensity ratio between the signals associated with C═O stretching (1730 cm^{-1}) and C—H bending in CH_2 for cellulose (2355 cm^{-1}). This ratio provides valuable insights into the extent of oxidation within the cellulose nanofibers [42]. Consistent with previous research findings, the intensity of the signal at 2355 cm^{-1} exhibited minimal changes regardless of the duration of isothermal stabilization. Therefore, this signal was utilized as the reference signal in the analysis, as it remained relatively unaffected throughout the stabilization process. Fig. 4c illustrates the relationship between the OD and the isothermal stabilization time. In general, longer stabilization times and higher amounts of oxidant were observed to result in an increase in OD [48]. In this study, a significant improvement in the OD was only observed after 5 h of holding time at 250 °C, with no significant improvement beyond 5 h of dwelling time. Bengtsson et al. [49] reported that lower dwelling time is required for the lignocellulosic materials to achieve a high oxidation degree, but a very slow heating rate of 0.2 °C/min was necessary during the process, making it inefficient and expensive in our case. As oxidation affects the crystalline structure [45], it is expected that both samples at 5 and 10 h of holding time would share the same properties after the carbonization process.

The impact of isothermal time on the crystalline structure of cellulose nanofibers was further investigated through XRD analysis. Fig. 5a illustrates the evolution of diffraction patterns from CA powder CA to CNFs after holding at 250 °C for 10 h. Three distinct peaks at $2\theta = 14.62$ (110), 16.29 (110), and 22.48 (200) confirmed the presence of cellulose I [50] in both cellulose acetate powder (CA) and nanofibers (CA NF). With an increase in holding time during the stabilization process, notable changes in the diffraction pattern were observed. A weak peak at $2\theta = 24.3$ was noticed for the heat-treated samples, and as the holding time increased to 10 h, distinct sharp peaks appeared, indicating the presence of a crystalline structure arranged in stacked layers [51]. After 5 h of holding time (CNF_5 and CNF_10), the crystalline peak split into two weaker peaks located at $2\theta = 20.1$ (110) and $2\theta = 21.53$ (200), suggesting the formation of the cellulose II structure [52]. The conversion of cellulose I to the more structurally stable cellulose II has been reported in previous studies via regeneration and mercerization using sodium hydroxide [53]. The presence of sodium hydroxide treatment during the deacetylation process might trigger the chain arrangement of cellulose I, and the prolonged holding time during stabilization is expected to stimulate the further formation of the stable antiparallel chain arrangement characteristic of cellulose II (Fig. 5b).

Interestingly, the distinct crystalline peak of cellulose II only appeared after dwelling for >5 h. This transition in cellulose crystalline structure in response to prolonged isothermal treatment is reported for

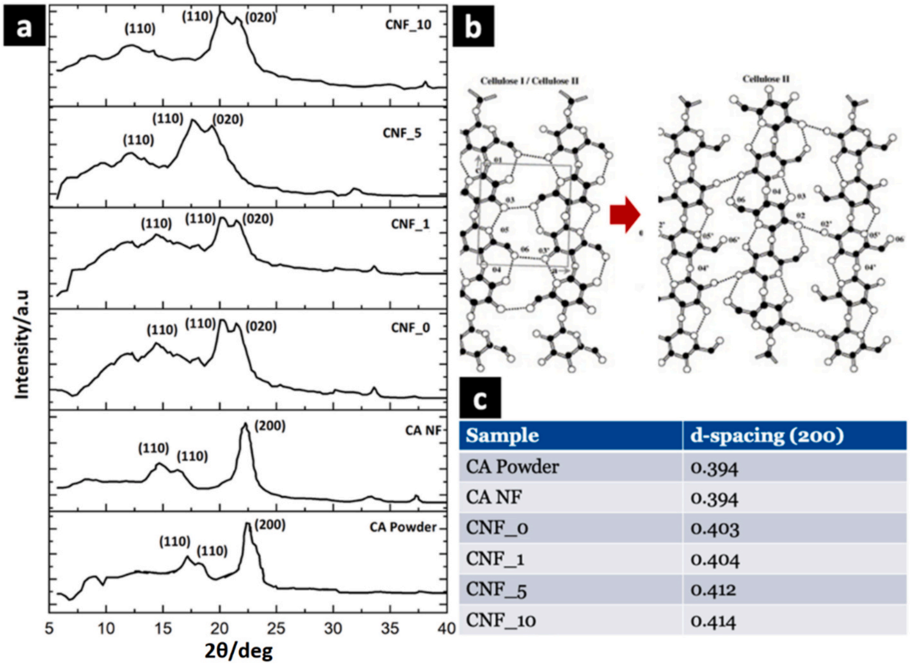

Sample	d-spacing (200)
CA Powder	0.394
CA NF	0.394
CNF_0	0.403
CNF_1	0.404
CNF_5	0.412
CNF_10	0.414

Fig. 5. XRD chromatogram of cellulose acetate NF, cellulose NF and different isothermal treated of cellulose NF.

the first time in this study, although the exact chemical pathways remain unclear. The presence of crystalline transition in samples between CA and CNFs could also be explained by changes in the d-spacing values in (002) planes (d002), as discussed by Ju et al. [54] in their work. The increasing value of d002 could be attributed to the formation of strong intermolecular hydrogen bonds in the cellulose II samples.

The transition of cellulose I to cellulose II after prolonged isothermal treatment can be further investigated through thermal behavior analysis, as shown in Fig. 6a. The transition to cellulose II has led to an increase in the onset degradation temperature from about 300 °C to 380 °C, and the remaining mass at 800 °C has significantly increased from approximately 4 % (CNF_0H) to 52 % (CNF_10H). In contrast, almost no residue remained on the cellulose acetate samples (powder and nanofiber) at 800 °C. The high mass yield observed in samples CNF_5 and CNF_10 indicates that these samples underwent a crystalline transformation, resulting in a higher degree of crystallinity after prolonged isothermal treatment. Numerous studies have reported that cellulosic materials with a high degree of crystallinity exhibit enhanced thermal stability [28,55]. Generally, thermal degradation initiates in the amorphous regions before progressing to the more crystalline structure. This explains the lower yield in samples CA powder, CA NF, and CNF_0H, as the cellulose I sample with predominantly amorphous structures is less heat resistant. Yue's studies support this finding, indicating that cellulose II exhibits better thermal stability than cellulose I.

Similar patterns were also observed when all the samples were subjected to pyrolysis in the tubular furnace under N_2 gas (Fig. 6b). The biomass yield (carbon nanofiber) of samples CA_NF_10H produced >60 % carbon nanofiber, which was higher than that reported during the TGA analysis. The 60 % recovery from the cellulosic precursors after pyrolysis is significantly higher than what has been previously reported in the literature [42]. The transition of cellulose crystalline structure has suppressed the formation of tar and volatiles, thereby maximizing the production of carbon nanofibers.

3.4. Surface morphology of cellulose-based carbon nanofiber

In addition to the formation of a fused ring system and crystalline degree, the production of carbon nanofibers can also be influenced by porosity and nanofiber size. Highly porous samples facilitate oxygen

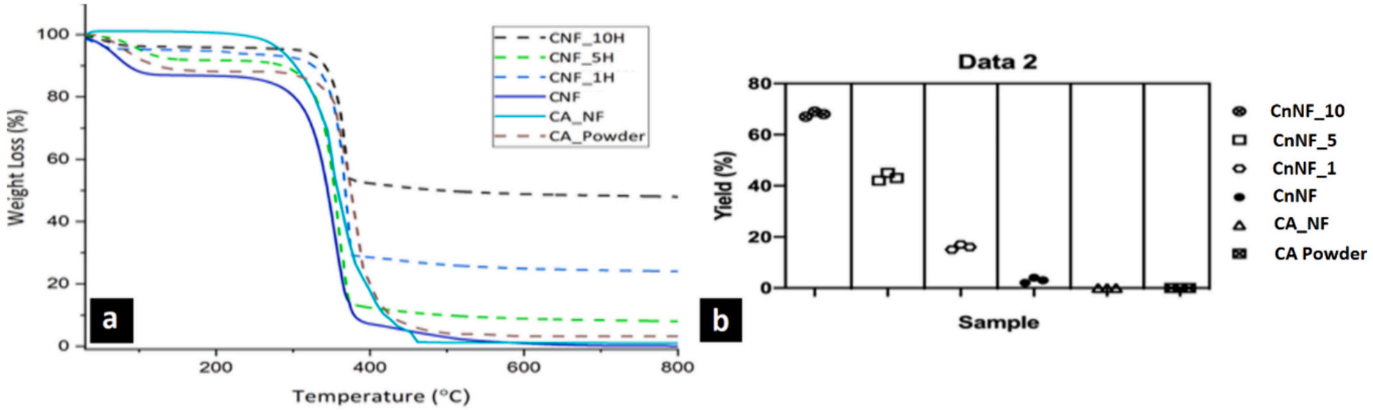

Fig. 6. (a). Thermogravimetric curves were recorded under a nitrogen atmosphere of CA powder, CA nanofiber, and Cellulose nanofiber with different holding times. (b). The yield of CA powder, CA nanofiber, and stabilized cellulose nanofiber.

diffusion into the core, leading to more homogeneous stabilization and higher carbon yield. Therefore, the effect of nanofiber size on carbon nanofiber formation was investigated using three different cellulose nanofibers ranging from 85 nm to 400 nm, prepared according to the prediction ternary graph presented in Section 3.2. The nanofibers were successfully obtained from CA at concentrations of 18 %, 23 %, and 25 % (wt) with fiber diameters of 80 nm, 100 nm, and 800 nm, respectively.

SEM images provide insights into the morphological features of both the cellulose nanofiber precursors and the resulting carbon nanofibers. Fig. 7 illustrates the SEM images and the nanofiber diameter distribution profile (insert) of cellulose nanofibers and carbon nanofibers prepared from different CA concentrations. After conversion into carbon nanofibers, there is a distinct reduction in nanofiber size by almost half. For instance, the nanofiber size of Ce_18% reduced from 85 nm to 46 nm (Fig. 7a), Ce_23% reduced from 140 nm to 80 nm (Fig. 7b), and Ce_25% reduced from 400 nm to 200 nm (Fig. 7c). This reduction in nanofiber size further confirms the loss of oxygen during the carbonization process. After 10 h of thermal stability at 250 °C, no fused nanofibers were observed in any of these cellulose nanofibers. The thermal stabilization transformed the cellulose nanofibers into a thermoset, enabling carbonization without losing their shape. In contrast, instant carbonization of cellulose nanofibers without stabilization induced fusion and structural collapsing. There were no distinct differences in carbon nanofiber yield between samples with different nanofiber sizes, possibly due to the homogenous stabilization resulting from the small diameter size. Moreover, the carbonization process stimulated physical crosslinking between the nanofibers, which is expected to improve the mechanical properties of the resulting carbon nanofibers.

Significantly higher carbon contents (ranging from 80 % to 90 %) were observed in the CnNFs samples compared to both CA and the cellulosic precursors (Table 2). This observation can be attributed to the formation of fused ring systems during the isothermal treatment. Subsequent pyrolysis at 800 °C under an inert atmosphere further converted the fused aromatic structures into a more ordered carbon structure by releasing non-carbon atoms (O and H) [46]. This phenomenon explains the impact of isothermal treatment on the carbon and oxygen content of the resulting carbon nanofibers. High carbon contents are desirable as they can enhance and facilitate the electrical conductivity of carbon nanofibers. The rearrangement of carbon elements into the sp^2 structure promotes pi-bond delocalization and the formation of free charge carriers, thereby increasing the electrical conductivity, making these carbon nanofibers suitable for various industrial applications [56].

The presence of inorganic impurities on carbon nanofibers has been reported in numerous studies that utilized biomass precursors for carbon nanofiber/fiber production [57]. Yuan et al. [58] demonstrated that the presence of impurities in carbonaceous materials significantly affects

Table 2
Elemental content of CA, spun CA, stabilized CNFs, and CnNFs. Data obtained from CHNS/O analyzer.

Elemental content (%)	C	H	N	S	O
CA powder	47.56 ± 0.45	5.98 ± 0.06	–	–	46.46 ± 0.49
Espun CA	47.75 ± 0.34	5.66 ± 0.02	–	–	46.59 ± 0.39
CNF_0	41.98 ± 0.54	5.96 ± 0.08	–	–	32.53 ± 0.52
CNF_1	42.03 ± 0.9	25.54 ± 0.12	–	–	32.43 ± 0.22
CNF_5	42.14 ± 0.65	21.17 ± 0.62	–	–	35.89 ± 0.51
CNF_10	41.94 ± 0.3	19.64 ± 0.25	–	–	38.42 ± 0.43
CnNF_1	80.10 ± 0.55	5.00 ± 0.03	–	–	14.90 ± 0.1
CnNF_5	89.70 ± 0.38	1.00 ± 0.01	–	–	9.30 ± 0.02
CnNF_10	90.12 ± 0.74	1.08 ± 0.01	–		8.80 ± 0.04

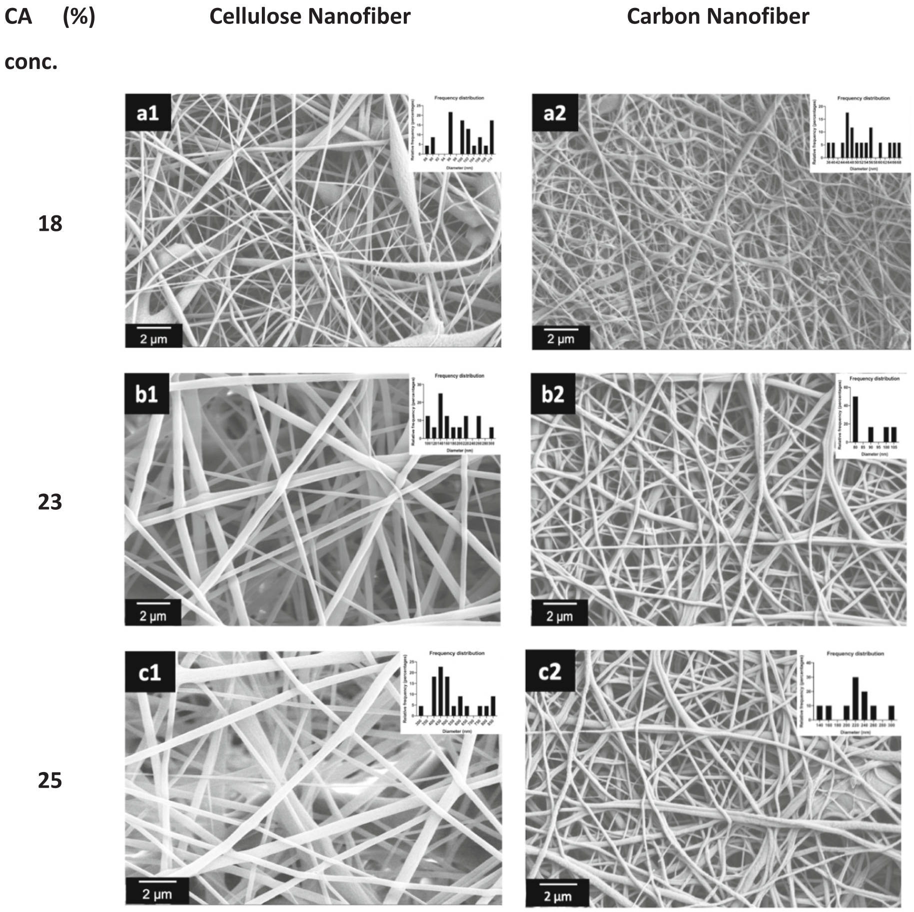

Fig. 7. Scanning electron microscopy images of (a1–c1) electrospun cellulose nanofiber after 10 h of isothermal treatment, (a2–c2) carbon nanofiber.

thermal stability and can cause a dramatic reduction in mechanical properties of up to 40 %. Therefore, proper washing after the deacetylation process and thermal stabilization is of paramount importance to avoid the presence of inorganic contaminants on the carbon nanofibers.

3.5. Surface area analysis

Table 3 presents the porous characteristics, including pore size distribution, total pore volume, and BET surface area, of all the samples. It is evident that the BET surface area of the carbon nanofibers exhibited a substantial increase, soaring from 0.1473 to 448 m^2/g, while the total pore volume increased from 0.002 to 0.5 cm^3/g compared to the cellulose acetate powder. These remarkable improvements in BET surface area and total pore volume in the carbon nanofibers can be attributed to the higher degree of crystallinity observed in the cellulose precursors, as confirmed by XRD analysis. Furthermore, the presence of pores in the carbon nanofibers, as verified by BJH and T-plot methods, also contributes to the enhanced surface area and pore volume. The high BET surface area and total pore volume of the carbon nanofibers render them highly desirable as they offer a larger number of active sites for surface functionalization. Additionally, these characteristics contribute to the improvement of CnNFs electroconductivity [59]. Although not the primary focus of the present work, the high surface area and pore volume have also enhanced electron transport onto the carbon surface, making them beneficial for improving electrochemical properties in energy storage applications [60].

Among the various carbon nanofibers, CnNF 18, which underwent a prolonged isothermal treatment of 10 h, demonstrated the highest BET-specific surface area of 445.402 m^2/g and a total pore volume of 0.430 cm^3/g. The significant increase in specific surface area and micropore volume in CnNF 18_10H was a result of the shrinkage of the ultrafine cellulose nanofiber from 85 nm to 46 nm during carbonization, promoting smaller fiber-to-fiber distances [57]. Additionally, the increase in cross-linking degree during the carbonization process also contributed to the rise in specific surface area and micropore volume [61]. Consequently, samples subjected to longer isothermal treatments exhibited higher specific surface area and micropore volume due to the formation of hyper cross-linking. Hasan et al. [61] reported that cross-linking not only improves the carbon yield but also enhances the tensile strength of the resulting carbon fibers.

3.6. Mechanical properties

The impact of isothermal heat treatment and carbon nanofiber size on the mechanical properties of cellulose-based CnNFs was investigated. It was observed that the tensile strength and Young's modulus increased with increasing isothermal treatment time, regardless of the nanofiber size [74]. For the CnNF_25 sample, prolonged isothermal treatment from 1 to 10 h during stabilization significantly increased the strength nearly 5-fold from 18.780 MPa to 123.808 MPa and led to about a 4-fold increase in Young's modulus, from 1.872 GPa to 9.592 GPa. Fig. 8a illustrates the tensile properties of the resulting CnNFs as a function of isothermal treatment time and nanofiber size. Despite no significant differences in the degree of oxidation and crystallinity between the treated precursors (CNF_5H and CNF_10H), the resulting CnNFs from CNF_10H exhibited superior strength and modulus. The prolonged treatment for 10 h promotes hyper-crosslinking formation between the graphite-type carbon layers [62], thus contributing to higher mechanical properties.

The tensile modulus of the resulting CnNFs in this study monotonically increases with isothermal treatment time. The results revealed that the tensile modulus of CnNF 25 increased from 1.846 GPa to 9.592 GPa when the isothermal time was prolonged from 1 h to 10 h. Qian et al. [63] reported that the tensile modulus of carbon fiber is influenced by microstructure properties and crystallinity degree, both of which are distinctively present in our resulting CnNFs. Therefore, the tensile modulus of CnNFs produced in this study exhibited better performance compared to most petroleum-based polymers CnNFs reported in the literature (Fig. 8b). To the best of our knowledge, the CnNFs prepared in this study demonstrated the highest tensile modulus and strength properties reported for carbon fibers prepared from biomasses.

3.7. Electrical conductivity

The electrical conductivity behaviors of the CnNFs are depicted in Fig. 9a. Overall, the conductivity properties of the CnNFs were significantly decreased with rapid isothermal treatment. As explained earlier, longer isothermal treatment induces crystalline transformation that affects the crystal structure and orientation, leading to higher electrical conductivity in samples subjected to longer dwelling times at 250 °C. Apart from isothermal time, CnNFs size also plays a crucial role in determining electrical conductivity [72]. While Ko et al. [73] reported a 2-fold increase in electrical conductivity as the diameter of nanofibers decreased from 260 nm to 140 nm, our study demonstrated a different pattern. The highest electrical conductivity was observed in CnNF 23_10H, with a conductivity reading of 1334 ± 69 μS/m, compared to CnNF 18_10H and CnNF 25_10H, which exhibited 485 ± 32 and 107.65 ± 20 μS/m, respectively. The presence of beads and a broad range of nanofiber sizes in CnNF 18_10H precursors might contribute to the formation of surface flaws and voids during the carbonization process [63].

The electrical conductivity of carbon nanofibers increases with the rise in the d200 value, which reflects the crystallographic order in the CnNFs (Fig. 9b). Qian et al. [63] reported that efficient electron mobility along the nanofiber axis is attributed to the improvement of electrical conductivity in CnNFs samples with a high degree of crystallinity and

Table 3
Porous characteristics of CA, spun CA, stabilized CNFs, and CnNF.

Sample	Average pore size (nm)	Total pore volume (cm^3/g)	Micropore volume (cm^3/g)	Mesopore volume (cm^3/g)	BET surface Area (m^2/g)
CA powder	26.323 ± 0.5	0.002 ± 0.0001	0	0.002 ± 0.0005	0.147 ± 0.03
Espun CA_18	5.908 ± 0.01	0.330 ± 0.002	0.019 ± 0.0001	0.329 ± 0.023	118.380 ± 5.4
Espun CA_23	7.837 ± 0.02	0.293 ± 0.001	0.003 ± 0.0003	0.290 ± 0.018	40.109 ± 3.9
Espun CA_25	8.053 ± 0.01	0.278 ± 0.003	0	0.280 ± 0.002	30.146 ± 2.73
Espun Ce_18	1.805 ± 0.03	0.438 ± 0.002	0.034 ± 0.0001	0.404 ± 0.006	158.402 ± 8.32
Espun Ce_23	2.140 ± 0.02	0.246 ± 0.012	0.0001 ± 0.00001	0.245 ± 0.003	71.006 ± 6.93
Espun Ce_25	3.915 ± 0.05	0.234 ± 0.011	0	0.242 ± 0.01	49.874 ± 8.03
CnNF_18_1	1.532 ± 0.01	0.448 ± 0.009	0.0003 ± 0.00001	0.447 ± 0.093	111.843 ± 10.1
CnNF_18_5	1.915 ± 0.008	0.494 ± 0.008	0.025 ± 0.0009	0.469 ± 0.007	128.613 ± 7.35
CnNF_18_10	0.915 ± 0.001	0.464 ± 0.004	0.100 ± 0.006	0.430 ± 0.009	448.402 ± 25.2
CnNF_23_1	2.837 ± 0.005	0.293 ± 0.004	0	0.296 ± 0.017	70.109 ± 12.94
CnNF_23_5	2.531 ± 0.001	0.262 ± 0.002	0.002 ± 0.0009	0.261 ± 0.0026	90.451 ± 3.1
CnNF_23_10	2.232 ± 0.002	0.248 ± 0.025	0.003 ± 0.00045	0.244 ± 0.001	101.678 ± 4.12
CnNF_25_1	3.805 ± 0.005	0.002 ± 0.0001	0	0.002 ± 0.0001	78.874 ± 2.03
CnNF_25_5	3.053 ± 0.001	0.003 ± 0.0009	0	0.003 ± 0.00001	80.146 ± 8.12

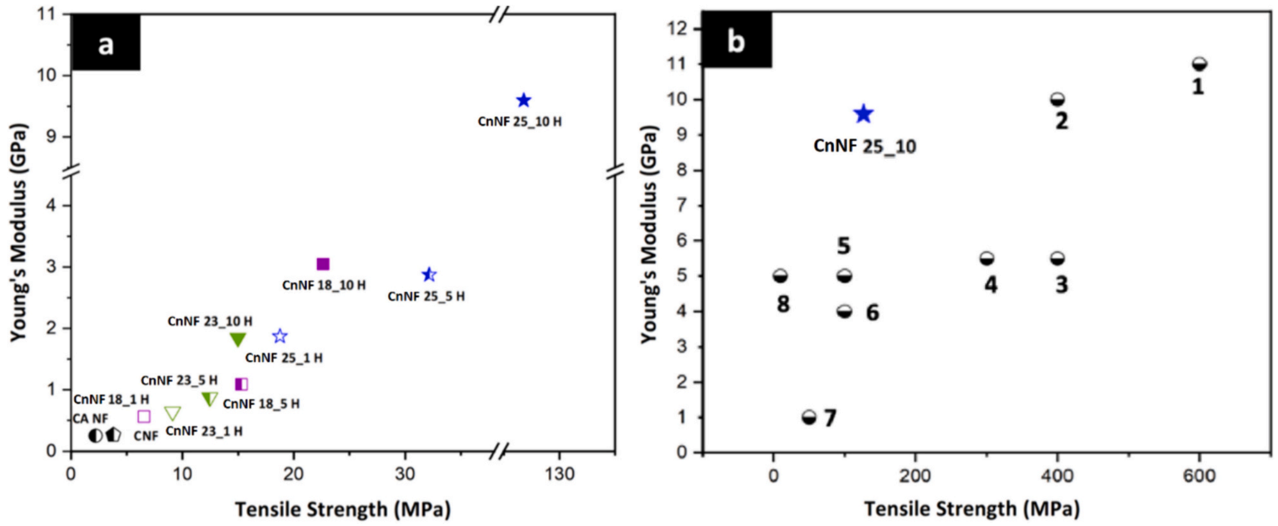

Fig. 8. Mechanical properties of (a). CA NF, CNFs, and cellulosic-based CnNFs are made by different isothermal treatment times and precursor diameters. Stars: CnNFs diameter (200 nm); Square: Thin CnNFs (80 nm) and inverted triangle: Ultra-thin CnNFs (46 nm). (b). Cellulosic-based CnNFs produced in group (Blue star) compared with those PAN-based CnNFs (half-filled circle) (1: [64]; 2: [65]; 3: [66]; 4: [67]; 5: [68]; 6: [69]; 7: [70]; 8: [71]) reported in the literature review. (For interpretation of the references to colour in this figure legend, the reader is referred to the web version of this article.)

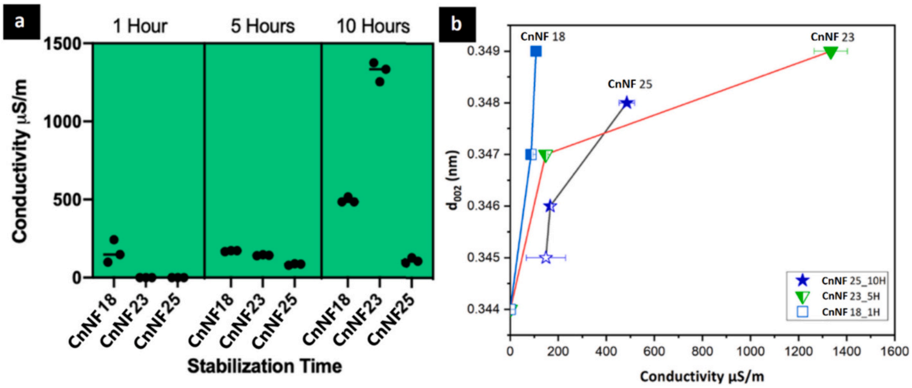

Fig. 9. (a). Electroconductivity of CnNFs with different isothermal treatment times. (b) Relationship between CnNFs and structural parameters d200.

orientation after prolonged isothermal treatment and high-temperature graphitization during the carbonization process. All the CnNFs samples demonstrated an enhancement in crystalline degree and electrical conductivity as the isothermal treatment time increased. However, the possibility of the presence of point defects and crystal impurities inhibited efficient electron transport within CnNF 18, despite its advantage of having a smaller nanofiber size. The electrical conductivity of CnNFs was found to be scaled with the tensile modulus; therefore, the samples with 10 h of prolonged isothermal treatment displayed the highest values in both electrical conductivity and tensile modulus for each nanofiber size.

4. Conclusions

The conversion of sugarcane biomass into high-modulus cellulose nanofibers presents a promising and sustainable approach for repurposing biowaste materials and generating high-value-added products. In this study, we successfully demonstrated the electrospinning of high acetyl cellulose acetate (CA) nanofibers derived from sugarcane bagasse, shedding light on their electrospinnability limits and the resulting control over nanofiber diameter (ranging from 80 nm for ultrathin, 200 nm for thin, to 800 nm for thick fibers).A key discovery of this research was the significant influence of prolonged isothermal treatment on the cellulose crystalline structure, profoundly impacting the properties of the resulting CnNFs. Optimization of isothermal dwelling time enhanced CnNFs carbon yield, increased specific surface area, and improved mechanical properties, yielding high-modulus CnNFs with superior tensile strength. These properties surpassed those of most petroleum-based polymer-derived CnNFs in existing literature, rendering them highly attractive for diverse applications in advanced materials and composites. Moreover, CnNFs produced from sugarcane bagasse exhibited a highly ordered microstructure and a high degree of crystallinity, augmenting their performance as reinforcement materials. The well-defined crystalline structure bolstered mechanical properties, positioning CnNFs as compelling candidates to replace or complement conventional synthetic reinforcements. Our study underscored the significance of high-temperature graphitization in enhancing the electrical conductivity of CnNFs. Controlled graphitization at elevated temperatures significantly improved electrical conductivity, concurrent with increases in d002 values and the degree of crystallinity. This heightened electrical conductivity unveiled novel opportunities for applications in conductive materials, energy storage devices, and functional coatings.

In conclusion, our research offers valuable insights into electrospinning high acetyl cellulose acetate nanofibers from sugarcane bagasse, facilitating the efficient and sustainable utilization of agricultural waste as a valuable feedstock for advanced materials. The amalgamation of enhanced mechanical properties, electrical conductivity, and controlled nanofiber diameter positions these CnNFs as highly desirable across a spectrum of applications in electronics, biomedicine, and environmental protection.

CRediT authorship contribution statement

Tamrin Nuge: Writing – review & editing, Writing – original draft, Visualization, Validation, Resources, Methodology, Investigation, Formal analysis, Data curation, Conceptualization. **Mahyar Fazeli:** Writing – review & editing, Writing – original draft, Visualization, Validation, Supervision, Methodology, Investigation, Conceptualization. **Hossein Baniasadi:** Writing – review & editing, Writing – original draft, Visualization, Validation, Conceptualization.

Declaration of competing interest

The authors declare that they have no known competing financial interests or personal relationships that could have appeared to influence the work reported in this paper.

Data availability

Data will be made available on request.

Acknowledgment

We acknowledge the financial support of Ningbo S&T Bureau under the Collaboration Project (Project code: 2017D10030, 2017D10033) by the Faculty of Science and Engineering, University of Nottingham Ningbo Campus (UNNC), and lab support by the team members of the composite research group, UNNC. The authors would like to acknowledge the Competence Center for Materials Bioeconomy, FinnCERES, for their financial support.

References

[1] D. Yadav, F. Amini, A. Ehrmann, Recent advances in carbon nanofibers and their applications – a review, Eur. Polym. J. 138 (2020) 109963, https://doi.org/10.1016/j.eurpolymj.2020.109963.

[2] W. Li, M. Li, M. Wang, L. Zeng, Y. Yu, Electrospinning with partially carbonization in air: highly porous carbon nanofibers optimized for high-performance flexible lithium-ion batteries, Nano Energy 13 (2015), https://doi.org/10.1016/j.nanoen.2015.03.027.

[3] S. Bigdeli, S. Fatemi, Fast carbon nanofiber growth on the surface of activated carbon by microwave irradiation: a modified nano-adsorbent for deep desulfurization of liquid fuels, Chem. Eng. J. 269 (2015), https://doi.org/10.1016/j.cej.2015.01.059.

[4] Y. Xing, Y. Wang, C. Zhou, S. Zhang, B. Fang, Simple synthesis of mesoporous carbon nanofibers with hierarchical nanostructure for ultrahigh lithium storage, ACS Appl. Mater. Interfaces 6 (2014), https://doi.org/10.1021/am404988b.

[5] J.R. Magana, Y. V. Kolen'Ko, F.L. Deepak, C. Solans, R.G. Shrestha, J.P. Hill, K. Ariga, L.K. Shrestha, C. Rodriguez-Abreu, From Chromonic self-assembly to hollow carbon nanofibers: efficient materials in supercapacitor and vapor-sensing applications, ACS Appl. Mater. Interfaces 8 (2016). doi:https://doi.org/10.1021/acsami.6b09819.

[6] F.J. García-Mateos, R. Ruiz-Rosas, J.M. Rosas, J. Rodríguez-Mirasol, T. Cordero, Controlling the composition, Morphology, Porosity, and Surface Chemistry of Lignin-Based Electrospun Carbon Materials, Front Mater 6 (2019) 114, https://doi.org/10.3389/fmats.2019.00114.

[7] Y. Zhang, F. Wang, H. Zhu, L. Zhou, X. Zheng, X. Li, Z. Chen, Y. Wang, D. Zhang, D. Pan, Preparation of nitrogen-doped biomass-derived carbon nanofibers/graphene aerogel as a binder-free electrode for high performance supercapacitors, Appl. Surf. Sci. 426 (2017), https://doi.org/10.1016/j.apsusc.2017.07.127.

[8] D. Wang, S. Dong, A. Ashour, X. Wang, L. Qiu, B. Han, Biomass-derived nanocellulose-modified cementitious composites: a review, Materials Today Sustainability 18 (2022), https://doi.org/10.1016/j.mtsust.2022.100115.

[9] X. Luo, S. Chen, T. Hu, Y. Chen, F. Li, Renewable biomass-derived carbons for electrochemical capacitor applications, SusMat 1 (2021), https://doi.org/10.1002/sus2.8.

[10] J. Yan, Y. Huang, Y. Zhang, W. Peng, S. Xia, J. Yu, B. Ding, Facile synthesis of bimetallic fluoride heterojunctions on defect-enriched porous carbon nanofibers for efficient ORR catalysts, Nano Lett. 21 (2021), https://doi.org/10.1021/acs.nanolett.1c00242.

[11] R. Awad, A. Haghighat Mamaghani, Y. Boluk, Z. Hashisho, Synthesis and characterization of electrospun PAN-based activated carbon nanofibers reinforced with cellulose nanocrystals for adsorption of VOCs, Chem. Eng. J. 410 (2021) 128412, https://doi.org/10.1016/j.cej.2021.128412.

[12] M. Fazeli, X. Liu, C. Rudd, The effect of waterborne polyurethane coating on the mechanical properties of epoxy-based composite containing recycled carbon fibres, Surfaces and Interfaces 29 (2022) 101684, https://doi.org/10.1016/j.surfin.2021.101684.

[13] R. Schierholz, D. Kröger, H. Weinrich, M. Gehring, H. Tempel, H. Kungl, J. Mayer, R.-A. Eichel, The carbonization of polyacrylonitrile-derived electrospun carbon nanofibers studied by in situ transmission electron microscopy, RSC Adv. 9 (2019) 6267–6277, https://doi.org/10.1039/C8RA10491C.

[14] B. Maddah, M. Soltaninezhad, K. Adib, M. Hasanzadeh, Activated carbon nanofiber produced from electrospun PAN nanofiber as a solid phase extraction sorbent for the preconcentration of organophosphorus pesticides, Sep. Sci. Technol. 52 (2017) 700–711, https://doi.org/10.1080/01496395.2016.1221432.

[15] E.J. Ra, E. Raymundo-Piñero, Y.H. Lee, F. Béguin, High power supercapacitors using polyacrylonitrile-based carbon nanofiber paper, Carbon N Y 47 (2009) 2984–2992, https://doi.org/10.1016/j.carbon.2009.06.051.

[16] M. Syduzzaman, A. Hassan, H.R. Anik, I.S. Tania, T. Ferdous, F.F. Fahmi, Unveiling new frontiers: Bast fiber-reinforced polymer composites and their mechanical properties, Polym. Compos. 44 (2023), https://doi.org/10.1002/pc.27661.

[17] M. Fazeli, S. Islam, H. Baniasadi, R. Abidnejad, I. Schlapp-Hackl, M. Hummel, J. Lipponen, Exploring the potential of regenerated Ioncell fiber composites: a sustainable alternative for high-strength applications, Green Chem. 26 (2024) 6822–6835, https://doi.org/10.1039/D3GC03637E.

[18] M. Fazeli, Development of Hydrophobic Thermoplastic Starch Composites. https://pantheon.ufrj.br/handle/11422/7843, 2018. (Accessed 17 July 2023).

[19] L. Bao, C. Xie, J. Shi, Y. Teramoto, Development of lignin-based carbon foam for use as an FRP sandwich core material, Polym. Compos. 42 (2021), https://doi.org/10.1002/pc.25853.

[20] M. Fazeli, R.A. Simão, The effect of cellulose nanofibers on the properties of starch biopolymer, Macromol. Symp. 380 (2018) 1800110, https://doi.org/10.1002/masy.201800110.

[21] M. Fazeli, R.A. Simão, Preparation and characterization of starch composites with cellulose nanofibers obtained by plasma treatment and ultrasonication, Plasma Processes Polym. 16 (2019), https://doi.org/10.1002/ppap.201800167.

[22] M. Fazeli, M. Keley, E. Biazar, Preparation and characterization of starch-based composite films reinforced by cellulose nanofibers, Int. J. Biol. Macromol. 116 (2018) 272–280, https://doi.org/10.1016/j.ijbiomac.2018.04.186.

[23] J.P. Florez, M. Fazeli, R.A. Simão, Preparation and characterization of thermoplastic starch composite reinforced by plasma-treated poly (hydroxybutyrate) PHB, Int. J. Biol. Macromol. 123 (2019) 609–621, https://doi.org/10.1016/j.ijbiomac.2018.11.070.

[24] M. Mujtaba, L. Fernandes Fraceto, M. Fazeli, S. Mukherjee, S.M. Savassa, G. Araujo de Medeiros, A. do Espírito Santo Pereira, S.D. Mancini, J. Lipponen, F. Vilaplana, Lignocellulosic biomass from agricultural waste to the circular economy: a review with focus on biofuels, biocomposites and bioplastics, J. Clean. Prod. 402 (2023). doi:https://doi.org/10.1016/j.jclepro.2023.136815.

[25] M. Fazeli, F. Fazeli, T. Nuge, O. Abdoli, S. Moghaddam, Study on the preparation and properties of polyamide/chitosan nanocomposite fabricated by electrospinning method, J. Polym. Environ. 30 (2022), https://doi.org/10.1007/s10924-021-02229-9.

[26] M. Ago, J.E. Jakes, L. Johansson, S. Park, O.J. Rojas, Interfacial Properties of Lignin-Based Electrospun Nanofibers and Films Reinforced with Cellulose Nanocrystals (2012), https://doi.org/10.1021/am302008p.

[27] M. Keley, M. Fazeli, R.A. Simão, F.P. Duda, Development of Superhydrophobic surfaces via isotropic etching and plasma sputter deposition, Ceramics in Modern Technologies XX (2018), https://doi.org/10.29272/cmt.2018.0002.

[28] M. Fazeli, J.P. Florez, R.A. Simão, Improvement in adhesion of cellulose fibers to the thermoplastic starch matrix by plasma treatment modification, Compos B Eng 163 (2019) 207–216, https://doi.org/10.1016/j.compositesb.2018.11.048.

[29] Y.G. Ko, U.S. Choi, Gelation of natural polymer dispersed suspensions under electric field, Soft Matter 8 (2012) 253–259, https://doi.org/10.1039/C1SM06400B.

[30] T. Kawabata, Y. Matsuo, Role of acetyl group on proton conductivity in chitin system, J. Mater. 5 (2019) 258–263, https://doi.org/10.1016/j.jmat.2019.02.010.

[31] N. Angel, L. Guo, F. Yan, H. Wang, L. Kong, Effect of processing parameters on the electrospinning of cellulose acetate studied by response surface methodology, J Agric Food Res 2 (2020) 100015, https://doi.org/10.1016/j.jafr.2019.100015.

[32] S.O. Han, J.H. Youk, K.D. Min, Y.O. Kang, W.H. Park, Electrospinning of cellulose acetate nanofibers using a mixed solvent of acetic acid/water: effects of solvent composition on the fiber diameter, Mater. Lett. 62 (2008) 759–762, https://doi.org/10.1016/j.matlet.2007.06.059.

[33] C. Appaw, S.A. Khan, R.D. Gilbert, J.F. Kadla, Sol-gel Transition of Cellulose Acetate in a Mixed Solvent System, In: Appita Conference and Exhibition (59th : 2005 : Auckland, N.Z.). 59th Appita Annual Conference and Exhibition: Incorporating the 13th ISWFPC (International Symposium on Wood, Fibre and Pulping Chemistry), Auckland, New Zealand, 16–19 May 2005: Proceed, 2021. doi:https://doi.org/10.3316/informit.342933557030202.

[34] F.A. Sheikh, M.A. Beigh, A.S. Qadir, S.H. Qureshi, H. Kim, Hydrophilically modified poly(vinylidene fluoride) nanofibers incorporating cellulose acetate fabricated by colloidal electrospinning for future tissue-regeneration applications, Polym. Compos. 40 (2019), https://doi.org/10.1002/pc.24910.

[35] M. Mulder, MEMBRANE PREPARATION | phase inversion membranes, in: I.D.B.T.-E. of S.S. Wilson (Ed.), Encyclopedia of Separation Science, Academic Press, Oxford, 2000: pp. 3331–3346. doi:https://doi.org/10.1016/B0-12-226770-2/05271-6.

[36] S. Neves, C. ~R. Leal, M. ~T. Cidade, Experimental Results on Electrorheology of Liquid Crystalline Polymer Solutions, in: A. Co, G.L. Leal, R.H. Colby, A.J. Giacomin (Eds.), The XV International Congress on Rheology, 2008: pp. 1429–1431. doi:https://doi.org/10.1063/1.2964598.

[37] M. Erencia, F. Cano, J.A. Tornero, M.M. Fernandes, T. Tzanov, J. Macanás, F. Carrillo, Electrospinning of gelatin fibers using solutions with low acetic acid concentration: effect of solvent composition on both diameter of electrospun fibers and cytotoxicity, J. Appl. Polym. Sci. 132 (2015) 1–11, https://doi.org/10.1002/app.42115.

[38] M. Hoque, T. Nuge, T.K. Yeow, N. Nordin, Electrospinning of gelatin nanofibre: current trends in tissue engineering applications, J Appl Mech Eng 02 (2013) 9873, https://doi.org/10.4172/2168-9873.1000e122.

[39] M. Erencia, F. Cano, J.A. Tornero, J. Macanas, F. Carrillo, Resolving the electrospinnability zones and diameter prediction for the electrospinning of the gelatin/water/acetic acid system, Langmuir 30 (2014) 7198–7205.

[40] K.A. Le, C. Rudaz, T. Budtova, Phase diagram, solubility limit and hydrodynamic properties of cellulose in binary solvents with ionic liquid, Carbohydr. Polym. 105 (2014) 237–243, https://doi.org/10.1016/j.carbpol.2014.01.085.

[41] K.Y. Lee, F. Quero, J.J. Blaker, C.A.S. Hill, S.J. Eichhorn, A. Bismarck, Surface only modification of bacterial cellulose nanofibres with organic acids, Cellulose 18 (2011) 595–605, https://doi.org/10.1007/s10570-011-9525-z.

[42] N. Byrne, R. De Silva, Y. Ma, H. Sixta, M. Hummel, Enhanced stabilization of cellulose-lignin hybrid filaments for carbon fiber production, Cellulose 25 (2018) 723–733, https://doi.org/10.1007/s10570-017-1579-0.

[43] A.J. Stamm, Thermal degradation of wood and cellulose, Ind. Eng. Chem. 48 (1956) 413–417, https://doi.org/10.1021/ie51398a022.

[44] M. Odalanowska, S. Borysiak, Influence of wood thermal modification on the supermolecular structure of polypropylene composites, Polym. Compos. 42 (2021), https://doi.org/10.1002/pc.25961.

[45] P. MITCHELL, Irreversible property changes of small loblolly pine specimens heated in air, nitrogen, or oxygen, Wood Fiber Sci. 20 (1988) 320–335.

[46] A.G. Dumanlı, A.H. Windle, Carbon fibres from cellulosic precursors: a review, J. Mater. Sci. 47 (2012) 4236–4250, https://doi.org/10.1007/s10853-011-6081-8.

[47] I. Pastorova, Cellulose char structure: a combined analytical pyrolysis gas chromatography-mass spectrometry, FTIR, and NMR study, Carbohydr Res 262 (n. d.) 27–47. https://doi.org/info:doi/.

[48] K.J. Nagarajan, N.R. Ramanujam, M.R. Sanjay, S. Siengchin, B. Surya Rajan, K. Sathick Basha, P. Madhu, G.R. Raghav, A comprehensive review on cellulose nanocrystals and cellulose nanofibers: pretreatment, preparation, and characterization, Polym. Compos. 42 (2021), https://doi.org/10.1002/pc.25929.

[49] A. Bengtsson, J. Bengtsson, M. Sedin, E. Sjöholm, Carbon fibers from lignin-cellulose precursors: effect of stabilization conditions, ACS Sustain. Chem. Eng. 7 (2019) 8440–8448, https://doi.org/10.1021/acssuschemeng.9b00108.

[50] M. Takahashi, H. Takenaka, Transition from cellulose i family to cellulose ii family, Polym. J. 19 (1987) 855–861, https://doi.org/10.1295/polymj.19.855.

[51] R.J. Moon, A. Martini, J. Nairn, J. Simonsen, J. Youngblood, Cellulose nanomaterials review: structure, properties and nanocomposites, Chem. Soc. Rev. 40 (2011) 3941–3994, https://doi.org/10.1039/c0cs00108b.

[52] S. Raymond, Aa. Kvick, H. Chanzy, The structure of cellulose II: a revisit, Macromolecules 28 (1995) 8422–8425, https://doi.org/10.1021/ma00128a063.

[53] M. Wada, M. Ike, K. Tokuyasu, Enzymatic hydrolysis of cellulose I is greatly accelerated via its conversion to the cellulose II hydrate form, Polym. Degrad. Stab. 95 (2010) 543–548, https://doi.org/10.1016/j.polymdegradstab. 2009.12.014.

[54] X. Ju, M. Bowden, E.E. Brown, X. Zhang, An improved X-ray diffraction method for cellulose crystallinity measurement, Carbohydr. Polym. 123 (2015) 476–481, https://doi.org/10.1016/j.carbpol.2014.12.071.

[55] M. Fazeli, S. Mukherjee, H. Baniasadi, R. Abidnejad, M. Mujtaba, J. Lipponen, J. Seppälä, O.J. Rojas, Lignin beyond the *status quo* : recent and emerging composite applications, Green Chem. 26 (2024) 593–630, https://doi.org/10.1039/D3GC03154C.

[56] X. Gu, C. Lai, F. Liu, W. Yang, Y. Hou, S. Zhang, A conductive interwoven bamboo carbon fiber membrane for Li–S batteries, J Mater Chem A Mater 3 (2015) 9502–9509, https://doi.org/10.1039/C5TA00681C.

[57] L. Szabó, X. Xu, T. Ohsawa, K. Uto, J. Henzie, I. Ichinose, M. Ebara, Ultrafine self-N-doped porous carbon nanofibers with hierarchical pore structure utilizing a biobased chitosan precursor, Int. J. Biol. Macromol. 182 (2021) 445–454, https://doi.org/10.1016/j.ijbiomac.2021.04.023.

[58] Q. Yuan, L. Li, Q. Li, F. Ding, Effect of metal impurities on the tensile strength of carbon nanotubes: a theoretical study, J. Phys. Chem. C 117 (2013) 5470–5474, https://doi.org/10.1021/jp4001847.

[59] M. Hakamada, T. Kuromura, Y. Chen, H. Kusuda, M. Mabuchi, Influence of porosity and pore size on electrical resistivity of porous aluminum produced by spacer method, Mater. Trans. 48 (2007) 32–36, https://doi.org/10.2320/matertrans.48.32.

[60] S.S. Lam, E. Azwar, W. Peng, Y.F. Tsang, N.L. Ma, Z. Liu, Y.-K. Park, E.E. Kwon, Cleaner conversion of bamboo into carbon fibre with favourable physicochemical and capacitive properties via microwave pyrolysis combining with solvent extraction and chemical impregnation, J. Clean. Prod. 236 (2019) 117692, https://doi.org/10.1016/j.jclepro.2019.117692.

[61] M. Ghafari, J.D. Atkinson, One-step hyper-cross-linking of porous styrenic polymers using dichloroalkane cross-linkers to maintain hydrophobicity, Polymer (Guildf) 116 (2017) 278–286, https://doi.org/10.1016/j.polymer.2017.03.082.

[62] Z. Wangxi, L. Jie, W. Gang, Evolution of structure and properties of PAN precursors during their conversion to carbon fibers, Carbon N Y 41 (2003) 2805–2812, https://doi.org/10.1016/S0008-6223(03)00391-9.

[63] X. Qian, J. Zhi, L. Chen, J. Zhong, X. Wang, Y. Zhang, S. Song, Evolution of microstructure and electrical property in the conversion of high strength carbon fiber to high modulus and ultrahigh modulus carbon fiber, Compos. Part A Appl. Sci. Manuf. 112 (2018) 111–118, https://doi.org/10.1016/j.compositesa.2018.05.030.

[64] Z. Xie, H. Niu, T. Lin, Continuous polyacrylonitrile nanofiber yarns: preparation and dry-drawing treatment for carbon nanofiber production, RSC Adv. 5 (2015) 15147–15153, https://doi.org/10.1039/c4ra16247a.

[65] L. Xiaojian, D. Martin, de S. e S.J. Martins, W.R. B., A. Seema, F. Stephan, H. Haoqing, S. Paul, G. Andreas, High strength in combination with high toughness in robust and sustainable polymeric materials, Science (1979) 366 (2019) 1376–1379. doi:https://doi.org/10.1126/science.aay9033.

[66] J.S. Youm, J.H. Kim, C.H. Kim, J.C. Kim, Y.A. Kim, K.S. Yang, Densifying and strengthening of electrospun polyacrylonitrile-based nanofibers by uniaxial two-step stretching, J. Appl. Polym. Sci. 133 (2016), https://doi.org/10.1002/app.43945.

[67] I.M. Alarifi, W.S. Khan, R. Asmatulu, Synthesis of electrospun polyacrylonitrile-derived carbon fibers and comparison of properties with bulk form, PloS One 13 (2018) e0201345.

[68] J.J. Ge, H. Hou, Q. Li, M.J. Graham, A. Greiner, D.H. Reneker, F.W. Harris, S.Z. D. Cheng, Assembly of well-aligned multiwalled carbon nanotubes in confined Polyacrylonitrile environments: electrospun composite nanofiber sheets, J. Am. Chem. Soc. 126 (2004) 15754–15761, https://doi.org/10.1021/ja048648p.

[69] H. Hou, J.J. Ge, J. Zeng, Q. Li, D.H. Reneker, A. Greiner, S.Z.D. Cheng, Electrospun Polyacrylonitrile nanofibers containing a high concentration of well-aligned multiwall carbon nanotubes, Chem. Mater. 17 (2005) 967–973, https://doi.org/10.1021/cm0484955.

[70] Z. Song, X. Hou, L. Zhang, S. Wu, Enhancing crystallinity and orientation by hot-stretching to improve the mechanical properties of electrospun partially aligned Polyacrylonitrile (PAN) nanocomposites, Materials 4 (2011), https://doi.org/10.3390/ma4040621.

[71] S. Deng, X. Liu, J. Liao, H. Lin, F. Liu, PEI modified multiwalled carbon nanotube as a novel additive in PAN nanofiber membrane for enhanced removal of heavy metal ions, Chem. Eng. J. 375 (2019) 122086, https://doi.org/10.1016/j.cej.2019.122086.

[72] F. Ko, H. Yang, Functional nanofibre: enabling material for the next generation smart textiles, Journal of Fiber Bioengineering and Informatics 1 (2008) 81–92, https://doi.org/10.3993/jfbi09200801.

[73] F.K. Ko, A. El-Aufy, H. Lam, A.G. Macdiarmid, 2 - Electrostatically Generated Nanofibres for Wearable Electronics, in: X.B.T.-W.E. and *P. Tao* (Ed.), Woodhead Publishing Series in Textiles, Woodhead Publishing, 2005: pp. 13–40. doi: https://doi.org/10.1533/9781845690441.13.

[74] M. Fazeli, S. Jayaprakash, H. Baniasadi, R. Abidnejad, J. Lipponen, Recycled carbon fiber reinforced composites: Enhancing mechanical properties through co-functionalization of carbon nanotube-bonded microfibrillated cellulose, Composites Part A: Applied Science and Manufacturing 180 (2024) 108097.

[75] H. Baniasadi, R. Abidnejad, M. Fazeli, J. Lipponen, J. Niskanen, E. Kontturi, J. Seppälä, O.J. Rojas, Innovations in hydrogel-based manufacturing: A comprehensive review of direct ink writing technique for biomedical applications, Advances in Colloid and Interface Science (2024) 103095.